MATERIALS CHEMISTRY
FRONTIERS

RESEARCH ARTICLE

View Article Online
View Journal | View Issue

Cite this: *Mater. Chem. Front.*, 2018, **2**, 993

Pressure-induced Mott-insulator–metal crossover at ambient temperature in an overexpanded fulleride†

Ruth H. Zadik,[a] Yasuhiro Takabayashi,[b] Ross H. Colman,[a] Gaston Garbarino[c] and Kosmas Prassides*[b]

Received 29th January 2018,
Accepted 13th March 2018

DOI: 10.1039/c8qm00048d

rsc.li/frontiers-materials

$Rb_{0.5}Cs_{2.5}C_{60}$ is a member of the family of face-centred-cubic (fcc)-structured alkali fullerides, A_3C_{60} (A = alkali metal) with a highly expanded lattice size. At ambient temperature and pressure, it is a Mott–Jahn–Teller insulator. However, upon cooling it exhibits first a crossover to an anomalous metallic state (Jahn–Teller metal) in the vicinity of 90 K followed next by a transition to a bulk superconductor with a transition temperature, T_c of 29.4 K. Here we study its structural and electronic response to the application of pressure. Synchrotron X-ray powder diffraction at ambient temperature shows that the same Mott-insulator–metal electronic state crossover can be induced through pressure application under isothermal conditions, as evidenced by a distinct broad symmetry-preserving compressibility anomaly, which sets in at ~0.4 GPa and extends to ~0.75 GPa. Complementary magnetic susceptibility measurements also reveal that the crossover temperature, T' tunable at ambient pressure through adjusting the dopant ratio to vary the unit cell volume, can be controlled through pressure application and be mapped onto the same global electronic phase diagram. The observed electronic response, as a function of both physical and 'chemical' pressure, is thus of the same electronic origin, namely the control of the bandwidth, W *via* outer wave function overlap of the constituent fulleride ions.

1. Introduction

Fulleride superconductors with stoichiometry A_3C_{60} crystallise as two different polymorphic phases with either body-centred-cubic-based (A15) or fcc structures.[1,2] Superconductivity occurs in competition with electronic ground states resulting from a fine balance between electron correlations and electron–phonon coupling in electronic phase diagrams strikingly similar to those of other unconventional superconducting materials such as the cuprates, the iron pnictides, and the heavy fermions.[3–5] In the A15-structured A_3C_{60} fullerides, superconductivity at the highest T_c (38 K) known for any molecular material emerges from a parent antiferromagnetic insulating (AFI) state – a Mott–Jahn–Teller insulator (MJTI) – upon pressurisation.[6,7] T_c scales in a dome-like relationship with V, the packing density or volume/C_{60}^{3-}, establishing the key role of strong electron correlations characteristic of unconventional superconductors other than fullerides.[1,6] The existence of a second fcc-structured A_3C_{60} polymorph allowed the investigation of the role of electron correlations and the competition of the AFI and superconducting states in two high-symmetry lattice packings at the same doping level. In fcc A_3C_{60}, T_c – which reaches a maximum value of 35 K – scales with V in an identical fashion to that of the A15 polymorph when normalized to proximity to the metal–insulator transition.[2] On the other hand, the magnetism of the parent AFI phases is controlled by the lattice packing – the fcc polymorph is geometrically frustrated and thus the onset temperature of antiferromagnetic order is suppressed by more than one order of magnitude relative to the bipartite A15 polymorph.[2] Notably for large values of V near the transition between the metallic and the Mott insulating phases, superconductivity is extremely robust and the upper critical magnetic field, H_{c2} of the fulleride superconductors reaches very large values as high as ~90 T – these are the highest known among three-dimensional isotropic superconductors.[8] Contrary to long-held beliefs, fullerides have therefore emerged as unconventional superconductors with a pairing interaction something other than simply the conventional BCS electron–phonon interaction.[1,2,6–12]

---

[a] *Department of Chemistry, Durham University, Durham DH1 3LE, UK*
[b] *WPI-Advanced Institute for Materials Research (WPI-AIMR), Tohoku University, Sendai 980-8577, Japan. E-mail: k.prassides@wpi-aimr.tohoku.ac.jp; Tel: +81 22 217 5953*
[c] *European Synchrotron Radiation Facility, Grenoble 38043, France*

† Electronic supplementary information (ESI) available: Refined parameters obtained by the Rietveld analysis of the synchrotron X-ray diffraction data of $Rb_{0.5}Cs_{2.5}C_{60}$ at 0.14 GPa and ambient temperature, comparison of the magnetic susceptibility data of $Rb_{0.5}Cs_{2.5}C_{60}$ collected inside and outside the pressure cell, and X-ray diffraction images of the $Rb_{0.5}Cs_{2.5}C_{60}$ sample at selected pressures. See DOI: 10.1039/c8qm00048d

In particular, we have recently probed extensively the Mott insulator–metal transition in the family of fcc-structured materials with composition, $Rb_xCs_{3-x}C_{60}$ ($0 \leq x \leq 3$).[9] Substitution of the smaller Rb^+ (1.52 Å) for the Cs^+ cation (1.67 Å) in Cs_3C_{60} mimics the effect of physical pressure and shifts the transition to ambient pressure. We found that the states at the two extremes of the control parameter, V (MJTI and normal metal) are straddled by an intermediate metallic phase where short-range quasi-localized electron behaviour associated with the intramolecular Jahn–Teller (JT) effect coexists with metallicity.[9] This state of matter, which we called a JT metal, is characterized by the fluctuating microscopic co-existence of localised and itinerant electrons and exhibits a strongly enhanced spin susceptibility relative to that of a conventional Fermi liquid, characteristic of the importance of strong electron correlations.

We now demonstrate using extremely fine control of applied external pressure in the low pressure regime of interest here that the crossover between the MJTI and JT metal phases in an expanded $Rb_xCs_{3-x}C_{60}$ phase with $x = 0.5$ can also be traversed purely through pressure application at ambient temperature, thereby firmly establishing that inter-fullerene spacing is the critical parameter controlling the electronic properties in these expanded cubic materials. The use of hydrostatic pressure and temperature as parameters to control unit cell volume, instead of alloying techniques, allows the fine alteration of experimental conditions, diminishing any effect from impurities which could influence the transition and enabling isobaric and isothermal sweeps.[10b,d] With decreasing volume, inter-C_{60}^{3-} orbital overlap increases, increasing the bandwidth W and thus reducing the ratio (U/W) (where U represents the on-site Coulomb repulsion), and in turn lowering correlation strength. The response of the $Rb_{0.5}Cs_{2.5}C_{60}$ unit cell metrics to variation in physical pressure and temperature is here investigated by high-pressure synchrotron X-ray powder diffraction at ambient T, and by high-pressure magnetic susceptibility measurements as a function of T.

2. Results and discussion

The pressure-dependent ambient-temperature synchrotron X-ray powder diffraction profiles of the sample could be modelled well up to ∼1 GPa using Rietveld analysis with a two-phase refinement. The sample comprised 70.6% fcc-structured $Rb_{0.5}Cs_{2.5}C_{60}$ at the lowest pressure (0.14 GPa) and 29.4% CsC_{60}; no other phases could be discerned (Fig. 1, top; Table S1, ESI†). The refinement technique and the structural model used were identical to those adopted in our earlier work on low-temperature high-pressure structural studies of the $Rb_xCs_{3-x}C_{60}$ series, as reported elsewhere.[9] At higher pressures, pressure-induced increased crystallinity of the sample led to deviations from true powder average being sampled and concurrent saturated regions appearing on the detector. This precluded analysis of these diffraction datasets by the Rietveld technique—instead Le Bail analysis for the fcc phase was employed above 1 GPa to reliably extract the evolution of the unit cell volume with pressure (Fig. 1, bottom). We emphasise that no evidence of symmetry breaking is evident throughout the whole pressure range under investigation.‡

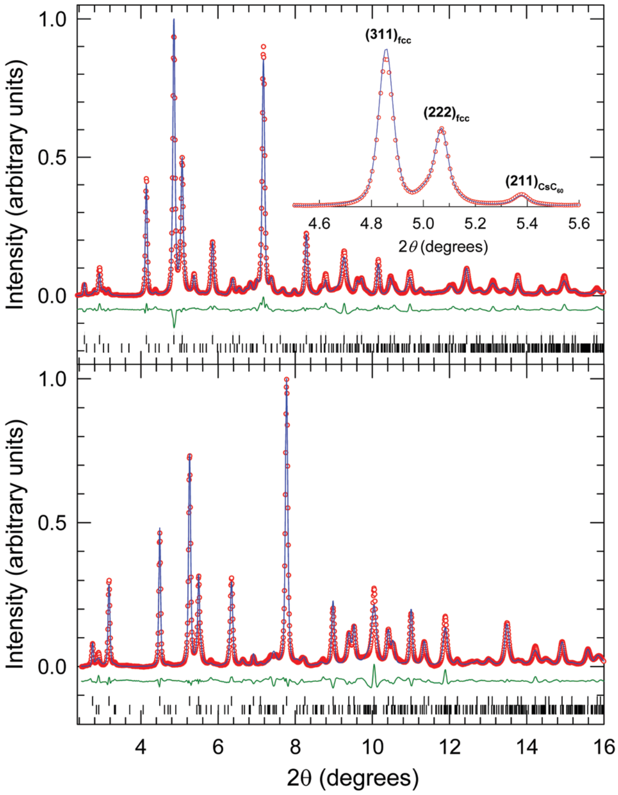

Fig. 1 High-pressure ambient-temperature synchrotron X-ray powder diffraction for $Rb_{0.5}Cs_{2.5}C_{60}$ (λ = 0.3738 Å). Final observed (red circles) and calculated (blue line) diffraction profiles at 0.14 GPa from Rietveld refinement (top) and at 12.1 GPa from Le Bail refinement (bottom). Green lines show the difference profiles, with ticks representing reflection positions for $Rb_{0.5}Cs_{2.5}C_{60}$ (70.61(9)%, upper line) and CsC_{60} (29.4(1)%, lower line). Inset (top): Expanded region of observed and calculated profiles at 0.14 GPa with reflections labelled by their (hkl) Miller indices.

The extracted pressure evolution of the unit cell volume of $Rb_{0.5}Cs_{2.5}C_{60}$ is presented in Fig. 2a. The compressibility shows no evidence of a pronounced discontinuity to 14.7 GPa; however, at the lowest pressures, a gradual upturn in the compressibility is revealed. This subtle effect emerged following a least-squares fit to the data with the Birch–Murnaghan equation-of-state (EoS),[13] based on the Taylor expansion of energy to third order in the Eulerian finite strain,[14] f_E: $P = 3K_0 f_E(1 + 2f_E)^{5/2}[1 + (3/2)(K_0' - 4)f_E]$, where K_0 is the zero-pressure isothermal bulk modulus, K_0' is its pressure derivative ($= \mathrm{d}K_0/\mathrm{d}P)_{P=0}$, V_0 is the unit cell volume at zero pressure, and $f_E = \frac{1}{2}[(V_0/V)^{2/3} - 1]$. When data in the pressure range 0.6–14.7 GPa are included in the fit, a distinct deviation between the fitted and experimentally

---

‡ The pressure evolution of the unit cell volume of the minority orthorhombic CsC_{60} phase is shown in Fig. S3 (ESI†). There is a clear compressibility anomaly with an onset at ∼2.6 GPa, evidence of a structural transition upon pressurization. This is in agreement with earlier high-pressure structural[21] and spectroscopic[22] work on phase-pure CsC_{60}. The absence of any anomaly in the low-pressure region (Fig. S3 inset) confirms that the presence of the minority impurity phase has no adverse effect on the physical response to pressure of the majority $Rb_{0.5}Cs_{2.5}C_{60}$ phase.

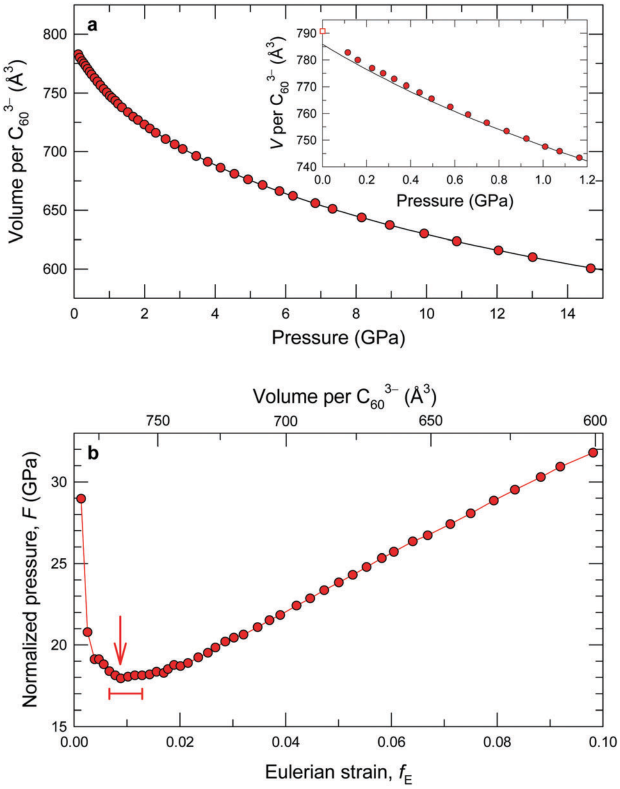

Fig. 2 (a) Pressure evolution of the C_{60} packing density, V (red circles) for $Rb_{0.5}Cs_{2.5}C_{60}$, at ambient temperature, up to an applied pressure of 14.7 GPa. The solid line is a fit to the third-order Birch–Murnaghan EoS in the range 0.6 to 14.7 GPa, with a zero-pressure isothermal bulk modulus, K_0 = 15.5(3), and its pressure derivative, K_0' = 11.2(2). Inset: Expanded view of the low-pressure data. The extrapolated ambient pressure volume, V_0 = 3144(2) Å^3, is smaller than that measured experimentally[9] (open square, 3163.26(3) Å^3). (b) Normalized pressure, F *vs.* Eulerian finite strain, f_E (lower axis) or packing density (upper axis) for $Rb_{0.5}Cs_{2.5}C_{60}$. The arrow and the horizontal bar mark the compression anomaly and its range around the packing density of ~765 Å^3/C_{60}^{3-}.

observed volumes at low pressures is unveiled (Fig. 2a inset). Significantly, as ambient P is approached from above, the experimental volume—while it deviates strongly from the value obtained from the EoS fit—tends towards that measured by high-resolution synchrotron X-ray powder diffractometry at ambient P,[9] corroborating our present findings. Recalling that the insulator-to-metal crossover at ambient P is marked by a unit cell volume decrease,[9] the present data indicate that an analogous volume change is occurring upon pressurisation—this is beyond the decrease expected upon applying pressure through reduction of inter-fullerene spacing. Therefore the metal–insulator boundary may be also traversed in these systems without necessitating access to low temperatures.

In order to attempt to unravel more clearly these subtle anomalies in volume compression, not easily apparent in the conventional V *vs.* P representation of Fig. 2a, the ambient T compression data of $Rb_{0.5}Cs_{2.5}C_{60}$ are replotted in Fig. 2b in terms of the Eulerian finite strain, f_E and the normalized pressure (or stress), $F = P/[3f_E(1 + 2f_E)^{5/2}]$, calculated by fixing V_0 to the value obtained from the Birch–Murnaghan EoS fit, depicted in Fig. 2a.[15] In the absence of any compressibility anomaly, F is a linear function of f_E with the intercept of the F *vs.* f_E plot equal to the bulk modulus, K_0 and the slope equal to $(3/2)K_0(K_0' - 4)$.[16] In the F *vs.* f_E plot (Fig. 2b), a clear deviation from linearity in F is indeed observed in the vicinity of a shallow minimum at $f_E' \sim 0.009$ ($P' \sim 0.5$ GPa) implying the occurrence of a pressure-induced isosymmetric change around a packing density of ~765 Å^3/C_{60}^{3-}. This is significantly smaller than the lattice packing density of $Rb_{0.5}Cs_{2.5}C_{60}$ at 90 K, ~779 Å^3/C_{60}^{3-}, where the transition occurs upon cooling at ambient P.

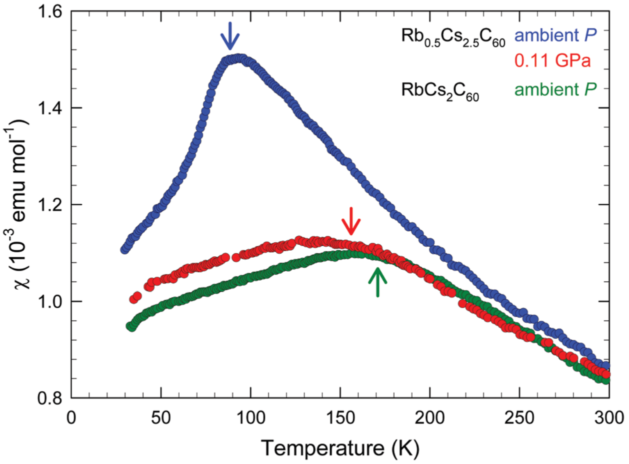

Fig. 3 Temperature dependence of the paramagnetic susceptibility, $\chi(T)$, of $Rb_{0.5}Cs_{2.5}C_{60}$ at ambient P (ref. 9) and at 0.11 GPa, and of $RbCs_2C_{60}$ at ambient P (ref. 9). Arrows mark the temperatures, T', at which maxima are observed.

A complementary study of the magnetic properties of $Rb_{0.5}Cs_{2.5}C_{60}$ in the normal state under pressure provided further validation of the implications of the structural results. The paramagnetic susceptibility, $\chi(T)$ of $Rb_{0.5}Cs_{2.5}C_{60}$ at ambient P follows the Curie–Weiss law at high temperatures with a negative Weiss temperature of −151 K but on further cooling it exhibits a well-defined cusp in the vicinity of $T' \sim 90$ K providing the signature of the insulator-to-metal crossover in direct correspondence with diffraction (Fig. 3 and Fig. S1, ESI†).[9] The cusp in $\chi(T)$ broadens and shifts to higher temperatures upon chemical pressurisation, which lowers the unit cell volume—this is clearly evident in the temperature variation of the paramagnetic susceptibility of the chemically-pressurised less-expanded $RbCs_2C_{60}$, in which a much broader crossover is found at $T' \sim 170$ K (Fig. 3).[9] We now find that an analogous effect occurs upon applying physical pressure§ to $Rb_{0.5}Cs_{2.5}C_{60}$—at an applied pressure of 0.11 GPa, the cusp shifts from ~90 K (ambient P) to ~157 K, while at the same time it becomes significantly broader, closely resembling the $\chi(T)$ curve of the $RbCs_2C_{60}$ analogue chemically-pressurised to comparable lattice size (Fig. 3).

---

§ The possibility that the physical behaviour observed is influenced by the presence of the pressure transmitting medium can be discarded by noting that the data collected with the sample inside the pressure cell before any pressure had been applied with the hydraulic oil press ram and the Daphne oil present are in excellent agreement with those measured in its absence with the sample in a quartz tube (Fig. S1, ESI†).

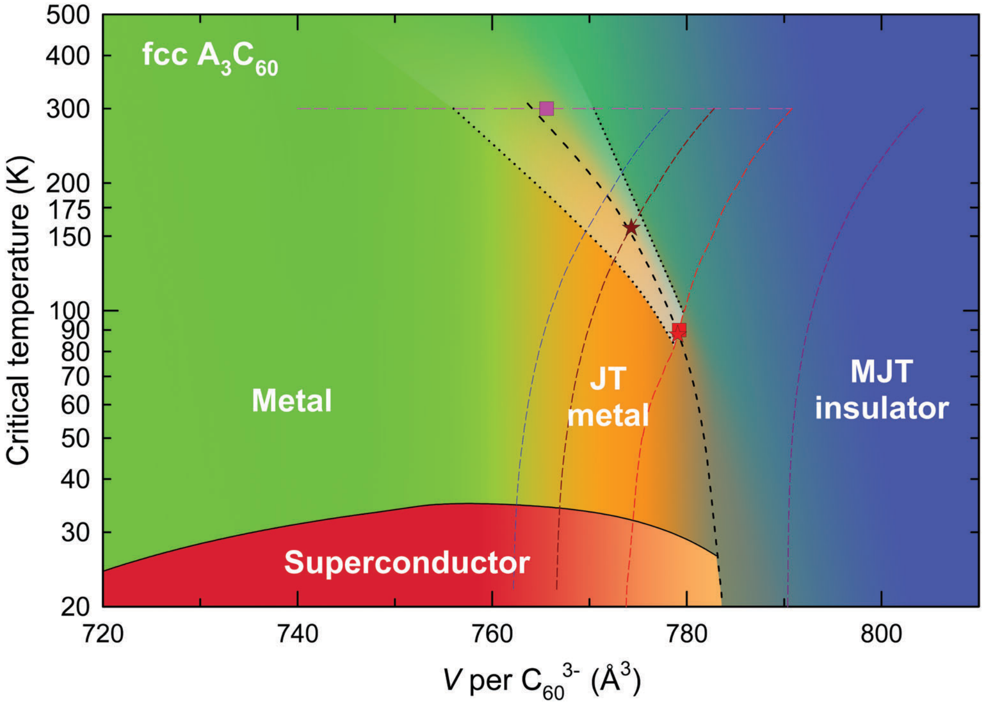

Fig. 4 Updated global electronic phase diagram of fcc-structured A_3C_{60} fullerides. The areas depicted in red, blue, orange, and green outline the superconducting, Mott–Jahn–Teller insulating (MJTI), Jahn–Teller metallic (JTM), and conventional metallic regimes of the phase diagram. The gradient-shaded area bounded by black dotted lines shows the crossover regime between insulator and metal with the black short-dashed line showing the dependence of the characteristic temperature, T' (synchrotron X-ray powder diffraction: squares; $\chi(T)$: stars) on V. Within the metallic (superconducting) regime, gradient shading from orange to green schematically illustrates the JTM to conventional metal (unconventional to weak-coupling BCS conventional superconductor) crossover. Downward dashed lines mark isobaric $V(T)$ tracks in order of decreasing V (from right to left) for Cs_3C_{60} at ambient P (violet), for $Rb_{0.5}Cs_{2.5}C_{60}$ at ambient P (red) and 0.11 GPa (brown),¶ and for $RbCs_2C_{60}$ at ambient P (blue). The horizontal dashed pink line marks the experimental isothermal $V(P)$ track for $Rb_{0.5}Cs_{2.5}C_{60}$.

The results are now considered in the context of the electronic phase diagram of fcc A_3C_{60} fullerides, focusing on the boundary between the MJT insulating and JT metallic phases. The demarcation line between these electronic phases of matter was constructed before by employing information under isobaric conditions from diffraction (negative volume change, $\Delta V = V_M - V_I$, below a characteristic temperature, T' in agreement with the virial theorem, which assigns itinerant electrons a lower volume), magnetometry (maximum in the temperature dependence of the magnetic susceptibility at T'), NMR spectroscopy (maximum in the temperature dependence of the ^{13}C spin–lattice relaxation rates divided by temperature, $1/^{13}T_1T$ at T'), and IR spectroscopy (step-like decrease in background transmittance below T').[9] A notable feature of the experimental results was that, in all cases, no phase co-existence regime was observed as it is necessitated by the first-order nature of the Mott transition and was verified experimentally before in other families of materials such as Cr-doped divanadium trioxide and the charge-transfer organic salts.[17] This implies that all samples studied are in the supercritical regime in the temperature-volume phase diagram where T' is higher than the critical end-point of the Mott transition, T_{cr} and a continuous second-order crossover between the phases occurs. This is a situation reminiscent of the liquid–gas transition and is consistent with the smearing out of the MJTI-JTM crossover over an increasingly broader temperature range as smaller values of V are accessed.

Fig. 4 shows the electronic phase diagram now extended to include the additional information derived by the present experiments on the $Rb_{0.5}Cs_{2.5}C_{60}$ composition. The ambient T volume at the characteristic pressure, P', shown by an arrow in Fig. 2b, is in good agreement with the trajectory of the phase boundary established through chemical pressurisation;[9] this provides excellent support of the present deduction that the observed compressibility anomaly is indeed a signature of the pressure-induced crossover from the insulating to the metallic phase. Moreover, the range of pressures over which the compression anomaly occurs (Fig. 2b) allows us to define the crossover between the two phases over a broad volume range under the isothermal conditions of the diffraction experiments, delineated by the dotted lines in Fig. 4. Very importantly, this approach can be extended to the information derived from the magnetic susceptibility data. At ambient P, the $\chi(T)$ cusp is fairly sharp implying a narrow range of co-existence. Upon pressurisation, the transition becomes more gradual. Notably the value of T' at 0.11 GPa falls perfectly on the existing trajectory,¶

¶ The isobaric $V(T)$ track for the $Rb_{0.5}Cs_{2.5}C_{60}$ composition at 0.11 GPa (Fig. 4) was derived by shifting the experimentally-determined ambient-P $V(T)$ track for the proximately sized $RbCs_2C_{60}$ composition so that the packing density at 300 K coincided with that measured experimentally for $Rb_{0.5}Cs_{2.5}C_{60}$ at 0.11 GPa—this assumes that the bulk modulus and its pressure coefficient vary little between the two cases. The inflexion point was calculated to coincide with the packing density at the temperature where the maximum in the $\chi(T)$ curve is observed.

while at the same time the derived crossover range fits well with the trend established by the high-pressure diffraction experiments.‖ Additional validation of our approach comes from the ambient P response of the chemically-pressurised $RbCs_2C_{60}$ composition whose lattice metrics lie very close to those of physically-pressurised $Rb_{0.5}Cs_{2.5}C_{60}$. As it is apparent in Fig. 4, the insulator-to-metal crossover observed in $RbCs_2C_{60}$ at ambient P mirrors that of $Rb_{0.5}Cs_{2.5}C_{60}$ at 0.11 GPa validating the conclusion that in these systems the electronic response as a function of both physical and chemical pressure can be mapped onto the same global electronic phase diagram.

3. Conclusions

In summary, we have presented ambient T synchrotron X-ray powder diffraction structural measurements on the ternary fcc-structured fulleride $Rb_{0.5}Cs_{2.5}C_{60}$ superconductor ($T_c = 29.4$ K at ambient P) at elevated pressures. By using extremely fine control of applied external pressure in the low-pressure regime, we have identified the occurrence of an isosymmetric structural transformation between the two competing insulating and metallic phases at ambient T. This crossover in electronic behaviour occurs over a broad pressure range (0.4–0.75 GPa) and maps perfectly well onto the global temperature-volume electronic phase diagram of fcc-structured fullerides built before on the basis of information derived at ambient P by varying the unit cell volume of the $Rb_xCs_{3-x}C_{60}$ family through the adjustment of the relative dopant ratio. Complementary isobaric magnetic susceptibility measurements help to enrich further the information available on the electronic phase crossover, defining a broad range of phase co-existence across the Mott-insulator–metal boundary and confirming that the materials are in the supercritical regime beyond the critical point of the first-order transition. There is a remarkable agreement between the effects of physical and chemical pressure on the bandwidth-controlled electronic properties of the fulleride family, explicitly illustrated in Fig. 4, confirming the defining role of the interfullerene separation, independently of the way that is tuned.

4. Experimental section

Fcc-structured $Rb_{0.5}Cs_{2.5}C_{60}$ was prepared by a solid–vapour annealing technique, as described elsewhere, with the specimen used here taken from sample I.[9]

Synchrotron X-ray powder diffraction experiments at high pressure were performed with the diffractometer on the ID27 beamline,[18] European Synchrotron Radiation Facility, Grenoble, France. A powder sample was loaded inside an argon-filled glovebox into a helium-gas-driven membrane diamond anvil cell (MDAC), with diamond culet diameter 600 μm, equipped with a stainless steel gasket with a hole 70 μm deep and 330 μm in diameter. Helium gas loaded in the MDAC was used as pressure medium, to achieve hydrostatic internal pressure conditions. The applied pressure was increased up to 14.7 GPa by controlling He gas pressure on the MDAC diaphragm, and internal pressure measured with the ruby fluorescence technique. Diffraction patterns were collected with a monochromatic X-ray beam ($\lambda = 0.3738$ Å) focused to 3×3 μm^2, using a MARCCD detector (165 mm diameter, 79.012 μm pixel size). Masking of the strong Bragg reflections of the diamond anvil and integration of the two-dimensional diffraction images (Fig. S2, ESI†) were performed with the FIT2D software,[19] with data analysis of the resulting one-dimensional diffraction profiles carried out with the GSAS suite of Rietveld analysis programs.[20] Pressure was carefully increased in small steps ($\delta P \sim 0.05$ GPa) in the low-P range to finely monitor the structural compression and correlate it with the corresponding temperature response at ambient P.

High-pressure SQUID magnetometry measurements were undertaken using an easyLab Technologies piston-cylinder high pressure cell (Mcell10), with high-purity Sn used as an *in situ* manometer and Daphne oil (easyLab) employed as pressure medium. Temperature-dependent magnetic susceptibility measurements were performed on a 26 mg sample, loaded in an argon-filled glovebox, at 3 and 5 T. $\chi(T)$ was obtained from the difference of the values at 5 and 3 T, to remove any contribution from ferromagnetic impurities, with an estimated core diamagnetic contribution also subtracted (see ref. 9). A correction was applied to account for the pressure losses during thermal cycling. A background contribution, determined through analogous measurements with the Mcell10 containing no sample or manometer, was subtracted from the raw data.

Conflicts of interest

There are no conflicts to declare.

Acknowledgements

This work was sponsored by the World Premier International (WPI) Research Center Initiative for Atoms, Molecules and Materials, Ministry of Education, Culture, Sports, Science and Technology of Japan. We acknowledge financial support from the Japan Society for the Promotion of Science (JSPS) under the Scientific Research on Innovative Areas 'π-System Figuration' (JP17H05139) and 'J-Physics' (No. JP15H05882) Projects and from the Mitsubishi Foundation. We thank the ESRF for access to synchrotron X-ray facilities.

Notes and references

1 A. Y. Ganin, Y. Takabayashi, Y. Z. Khimyak, S. Margadonna, A. Tamai, M. J. Rosseinsky and K. Prassides, *Nat. Mater.*, 2008, 7, 367.

‖ T' was defined as the intersection point of two linear fits to the experimental $\chi(T)$ data, collected at temperatures directly below and above the approximate maximum. The crossover range was then defined as the temperature range bound by the points where the higher- and lower-T linear fits diverge from the experimental data.

2 A. Y. Ganin, Y. Takabayashi, P. Jeglič, D. Arčon, A. Potočnik, P. J. Baker, Y. Ohishi, M. T. McDonald, M. D. Tzirakis, A. McLennan, G. R. Darling, M. Takata, M. J. Rosseinsky and K. Prassides, *Nature*, 2010, **466**, 221.

3 P. A. Lee, N. Nagaosa and X.-G. Wen, *Rev. Mod. Phys.*, 2006, **78**, 17.

4 Y. J. Uemura, *Nat. Mater.*, 2009, **8**, 253.

5 Q. Si and F. Steglich, *Science*, 2010, **329**, 1161.

6 Y. Takabayashi, A. Y. Ganin, P. Jeglič, D. Arčon, T. Takano, Y. Iwasa, Y. Ohishi, M. Takata, N. Takeshita, K. Prassides and M. J. Rosseinsky, *Science*, 2009, **323**, 1585.

7 G. Klupp, P. Matus, K. Kamarás, A. Y. Ganin, A. McLennan, M. J. Rosseinsky, Y. Takabayashi, M. T. McDonald and K. Prassides, *Nat. Commun.*, 2012, **3**, 912.

8 Y. Kasahara, Y. Takeuchi, R. H. Zadik, Y. Takabayashi, R. H. Colman, R. D. McDonald, M. J. Rosseinsky, K. Prassides and Y. Iwasa, *Nat. Commun.*, 2017, **8**, 14467.

9 R. H. Zadik, Y. Takabayashi, G. Klupp, R. H. Colman, A. Y. Ganin, A. Potočnik, P. Jeglič, D. Arčon, P. Matus, K. Kamarás, Y. Kasahara, Y. Iwasa, A. N. Fitch, Y. Ohishi, G. Garbarino, K. Kato, M. J. Rosseinsky and K. Prassides, *Sci. Adv.*, 2015, **1**, e1500059.

10 (*a*) Y. Ihara, H. Alloul, P. Wzietek, D. Pontiroli, M. Mazzani and M. Riccò, *Phys. Rev. Lett.*, 2010, **104**, 256402; (*b*) Y. Ihara, H. Alloul, P. Wzietek, D. Pontiroli, M. Mazzani and M. Riccò, *EPL*, 2011, **94**, 37007; (*c*) P. Wzietek, T. Mito, H. Alloul, D. Pontiroli, M. Aramini and M. Riccò, *Phys. Rev. Lett.*, 2014, **112**, 066401; (*d*) H. Alloul, P. Wzietek, T. Mito, D. Pontiroli, M. Aramini, M. Riccò, J. P. Itie and E. Elkaim, *Phys. Rev. Lett.*, 2017, **118**, 237601.

11 A. Potočnik, A. Y. Ganin, Y. Takabayashi, M. T. McDonald, I. Heinmaa, P. Jeglič, R. Stern, M. J. Rosseinsky, K. Prassides and D. Arčon, *Chem. Sci.*, 2014, **5**, 3008; A. Potočnik, A. Krajnc, P. Jeglič, Y. Takabayashi, A. Y. Ganin, K. Prassides, M. J. Rosseinsky and D. Arčon, *Sci. Rep.*, 2014, **4**, 4265; Y. Kasahara, Y. Takeuchi, T. Itou, R. H. Zadik, Y. Takabayashi, A. Y. Ganin, D. Arčon, M. J. Rosseinsky, K. Prassides and Y. Iwasa, *Phys. Rev. B: Condens. Matter Mater. Phys.*, 2014, **90**, 014413; Y. Takabayashi and K. Prassides, *Struct. Bonding*, 2016, **172**, 119; Y. Takabayashi and K. Prassides, *Philos. Trans. R. Soc., A*, 2016, **374**, 20150320; M. Menelaou, Y. Takabayashi, H. E. Okur, R. H. Zadik and K. Prassides, *Int. J. Mod. Phys. B*, 2018, **32**, 1840020.

12 J. E. Han, O. Gunnarsson and V. H. Crespi, *Phys. Rev. Lett.*, 2003, **90**, 167006; G. R. Darling, A. Y. Ganin, M. J. Rosseinsky, Y. Takabayashi and K. Prassides, *Phys. Rev. Lett.*, 2008, **101**, 136404; M. Capone, M. Fabrizio, C. Castellani and E. Tosatti, *Rev. Mod. Phys.*, 2009, **81**, 943; R. Akashi and R. Arita, *Phys. Rev. B: Condens. Matter Mater. Phys.*, 2013, **88**, 054510; Y. Murakami, P. Werner, N. Tsuji and H. Aoki, *Phys. Rev. B: Condens. Matter Mater. Phys.*, 2013, **88**, 125126; Y. Nomura, S. Sakai, M. Capone and R. Arita, *Sci. Adv.*, 2015, **1**, e1500568; H.-C. Jiang and S. Kivelson, *Phys. Rev. B: Condens. Matter Mater. Phys.*, 2016, **93**, 165406; N. Iwahara and L. F. Chibotaru, *Nat. Commun.*, 2016, **7**, 13093; S. Hoshino and P. Werner, *Phys. Rev. Lett.*, 2017, **118**, 177002.

13 F. Birch, *Phys. Rev.*, 1947, **71**, 809.

14 F. D. Stacey, B. J. Brennan and R. D. Irvine, *Geophys. Surv.*, 1981, **4**, 189.

15 R. Jeanloz and R. M. Hazen, *Am. Mineral.*, 1991, **76**, 1765.

16 R. J. Angel, *Rev. Mineral. Geochem.*, 2000, **41**, 35.

17 A. Jayaraman, D. B. McWhan, J. P. Remeika and P. D. Dernier, *Phys. Rev. B: Condens. Matter Mater. Phys.*, 1970, **2**, 3751; F. Kagawa, K. Miyagawa and K. Kanoda, *Nat. Phys.*, 2009, **5**, 880.

18 M. Mezouar, W. A. Crichton, S. Bauchau, F. Thurel, H. Witsch, F. Torrecillas, G. Blattmann, P. Marion, Y. Dabin, J. Chavanne, O. Hignette, C. Morawe and C. Borel, *J. Synchrotron Radiat.*, 2005, **12**, 659.

19 A. P. Hammersley, S. O. Svensson, M. Hanfland, A. N. Fitch and D. Häusermann, *High Pressure Res.*, 1996, **14**, 235.

20 A. C. Larson and R. B. von Dreele, *General Structure Analysis System (GSAS)*, Los Alamos National Laboratory Report LAUR 86-748, 2000.

21 K. Vavekis, DPhil thesis, University of Sussex, 1997; I. Margiolaki, DPhil thesis, University of Sussex, 2003.

22 J. Arvanitidis, K. Papagelis, I. Tsilika, G. Kanellis, S. Ves, G. A. Kourouklis, K. Tanigaki and K. Prassides, *Physica B*, 1999, **265**, 234.